Indian Journal of Chemical Technology
Vol. 31, July 2024, pp. 564-570
DOI: 10.56042/ijct.v31i4. 4026

Study of electrochemical behaviour of AZ91 Mg-based composites

Kamal Kant Singh* & Dharamvir Mangal
Mechanical Engineering Department, Gautam Buddha University, Greater Noida, Uttar Pradesh, India
*E-mail: kamalkantsingh.kc@gmail.com

Received 15 July 2023; accepted 15 May 2024

In this research study, electrochemical behaviour of AZ91/12Al_2O_3 and AZ91/12Al_2O_3/3TiC composites are investigated using different methods such as linear polarization resistance, electrochemical spectroscopy, noise measurements, and potential dynamic polarization curves. Both composites have been fabricated by using a two-step stir casting process. These composites include alumina (Al_2O_3) and TiC (titanium carbide) as reinforcing particles amalgamated with AZ91 Mg alloy. However, AZ91 Mg alloy depicts 9% of aluminium, 1% of zinc and rest is balance of pure magnesium, AZ91/12Al_2O_3 signifies AZ91 Mg alloy having 12 wt. % of alumina whereas AZ91/12Al_2O_3/3TiC indicates 3 wt. % of titanium carbide and 12 wt.% of Al_2O_3 in AZ91 Mg alloy. The conclusive result of these methods illustrate that AZ91/12Al_2O_3 composite exhibits high corrosion rate as compared to AZ91/3TiC/12Al_2O_3 composite due to high galvanizing effect (in between corrosive surface) of AZ91 Mg alloy and alumina particles. Lastly, the results of the electrochemical impedance of both composites illustrate the diffusion/adsorption type phenomenon.

Keywords: AZ91 Mg alloy, Alumina, Nyquist diagram, Polarization curves, SEM micrographs, Titanium carbide, Two-step stir casting process

Introduction

The demand and the usage of Mg-based matrix composites in automobile part design applications increases due to its light-weight and good strengthening properties. Mg-alloys have widely evolved as metal matrix composites because they exhibit low density, high corrosion resistance, and high mechanical strength[1-3]. Mg-matrix composites are eminently preferred in aero-designing applications such as airplane wings and cockpit panels[4,5]. The key drawback of magnesium and aluminium-zinc based alloys is their high rate of chemical reactivity which resists development in the field of designing applications[6,7]. Most significantly it is due to its unfavourable electrochemical behaviour. When alumina particles are reinforced with magnesium alloys, composites show improved results. It is due to its improved properties such as good wettability and specific strength which form a strong interface between the Mg-matrix and alumina[8]. Literature study reveals that the amalgamation of TiC as reinforcement with AZ91 Mg alloy also enhances the strengthening properties under high-temperature conditions[9].

Majorly, researchers target their study towards magnesium-based matrix composites rather than Al-based composites because of its wide possibilities. Most of the research studies have been focused to evaluate the tribological and immersion behaviour of Mg alloy-based composites. Dubey *et al.*[10] performed a corrosion study of AZ80 Mg alloy composites and examined the corrosion damage of Mg-composite surfaces due to the formation of a magnesium hydroxide corrosion layer. But when AZ80 and AZ91 Mg both composites have been compared, AZ91 Mg composites exhibit a high corrosion resistance as observed by Bahmani *et al.*[11]. The formation of $Mg_{17}Al_{12}$ i.e., beta phase network, and the existence of aluminium in AZ91 composite deteriorates (corroded) the surface of composites[11]. Beta phase and Al reacts with the atmosphere forms oxide layer which deteriorates the AZ91 composite surface and shows the significant corrosion effect. Aydin *et al.* [12] examined the immersion data values of AZ91 composites with TiC and compared with AZ91 alloy base material, by considering an electrochemical test. Their study demonstrated that the AZ91 Mg reinforced composite shows a slight positive change in corrosion rate with time as compared to the base matrix i.e. AZ91Mg alloy due to 2 times rapid growth corrosion rate around regional (outermost) surfaces of AZ91 composite in comparison to the AZ91 Mg alloy. Moreover, Odabasi *et al.*[13] demonstrated a fragile association between their interfaces and regional corrosion surfaces of Mg-based reinforced with TiC and ZrC composites. Tarasasanka *et al.* [14]

studied the corrosion resistance of AZ91 Mg/Alumina composites and observed that the rate of corrosion surpasses in AZ91 composites due to the development of a flimsy corrosion layer as compared to the AZ91 Mg alloy. Moreover, the study of Singh *et al*.[15] reported the immersion results of Mg-based hybrid composites in contrast with pure Mg when dipped in NaCl solution. According to their studies, the existence of alumina particles decreases the corrosion resistance of magnesium and progresses the corrosion effect with the rise of boron carbide (wt.%) particles. Their results also depict the galvanic corrosion rate in-between the Mg-matrix and B_4C reinforcement. Thus, the overall corrosion effect of AZ91 Mg composites surpasses. Aydin *et al*.[16] performed electrochemical experimentation of AZ91 hybrid composites in 3.5 wt.% NaCl immersion solution under ambient temperature and their results revealed that AZ91 alloy shows certain potential drops but AZ91 hybrid composites not representing potential drops. During anodic reaction under 3V in NaCl immersion solution for 30 min, the anti-corrosion behaviour of AZ91 hybrid composite specimens shows significant behaviour in comparison to the non-anodic reaction of the same specimens. Lastly, Singh *et al*. [17] observed the immersion behaviour of Mg composites reinforced with Cr in 3.5% NaCl solution. Their result signifies an increase in (corrosion) resistance with the rise of Cr wt.% reinforcement in Cr-reinforced composites. Metallographic observation of composite samples depicts galvanic activity around matrix-reinforcing interfaces as well as the formation of effluent corrosion films and thus improves the corrosion resistance of Cr-reinforced composites.

Thus from the above study, AZ91 Mg reinforced composites show anti-corrosion behaviour when reinforced with TiC, Alumina, Cr, Zr etc. Thereof, current research work has been focused to illustrate the corrosion resistance effect (by considering different electrochemical method) of AZ91/12Al_2O_3 (C1) having alumina as reinforcement and AZ91/12Al_2O_3/3TiC (C2) composites having TiC and alumina reinforcements.

Experimental Section

Table 1 shows the chemical composition of experimented AZ91 Mg alloy which shows the existence of Al and Zn as the key (alloying) elements with a balance of Mg. AZ91 composites fabricated by vacuum-based squeezed stir casting process having AZ91 as base matrix and TiC and Al_2O_3as reinforcing materials.

Initially, to eliminate the moisture and impurities from reinforcing particles, TiC and Al_2O_3 powders have been placed in an electric oven for pre-heating at 300^{o}C individually. Then under constant stirring, AZ91 matrix ingots have been placed in a vacuum-preheated furnace setup equipped with Argon + Sulphur hexafluoride (HF_6) cover gas to protect it from fire (as AZ91 Mg have oxidative property when burn in atmosphere). Then reinforcements (TiC + Al_2O_3) have been incorporated (through equipped reinforcing attachment) into AZ91-Mg molten melt (AZ91 Mg reach upto 850^{o}C) under constant stirring (455 rpm for 15 min) to attain a uniform distribution. After that, composite melt dropped into the mould by the bottom pouring method. In this method, a preheated (250^{o}C) small inclined platform was attached below the preheated furnace to maintain the composite melt temperature. Then melt dropped into the mould and instantaneously squeeze pressure (250 MPa) enforced by hydraulic press for 10 min to remove the residual deformities. After that fabricated composite specimens sliced out as per required ASTM standards as shown in the study of Singh *et al*. [18].

For the corrosion immersion test, C1 and C2 composites specimens were dipped and experimented in a 3.5% NaCl immersion solution under ambient temperature. An computer operated ACM potentiostat setup attached with Grammy PC4 300 potentiostat machine software (Spectro Analytical Labs Private Limited, Greater Noida) is used for LPR (linear polarization resistance) measurements and polarization curves. For the evaluation of polarization (curves) data values, setup includes a conventional 3-electrode glass cell integrated with an auxiliary rod (graphite electrode) and SCE (saturated electrode) under the sweep rate of 1mV/s for open circuit potential (E_{corr}) for the interval of -700 mV to 700 mV. Moreover, by using same setup, linear polarization resistance (LPR) measurements have been performed by polarizing. For polarizing

Table1 — Chemical distribution of AZ91 Mg alloy Matrix

Elements	Mg	Al	Zn	Mn	Si	Fe	Cu	Ni
Weight %	Balance	8.7	0.7	0.24	0.2	0.005	0.0015	0.001

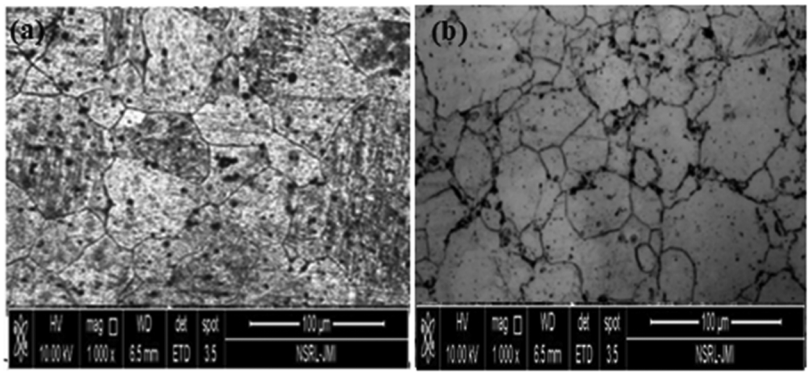

Fig. 1 — Polished microscopic images of (a) AZ91/12Al_2O_3 and (b) AZ91/3TiC/12Al_2O_3 composites

corrosion current density (I_{corr}) ofAZ91 composite specimens measured at a scanning rate of 1 mV/s for every 60 min in the duration of 24 h from +10 to -10 mV.

Corrosion current density can also be evaluated by considering Tafel extrapolation method with the interval of 250 mV when I_{corr} become stable. Another corrosion test i.e., electrochemical impedance spectroscopy (EIS) test have been performed by using same setup with an amplitude of 10 mv under a frequency interval of 0.1 Hz to 10 kHz using E_{corr}. Lastly, for electrochemical noise measurement (i.e., current and potential values) measured by using 2 identical working and reference electrodes simultaneously by recording current and potential fluctuations for 18 min at a sampling rate of 1 point/second. For evaluating the noise analysis, the initial step is to eliminate the drift of DC from actual noise data by considering the least square (fitting) method. Lastly, Rn (noise resistance or linear polarization resistance) was evaluated as the ratio of potential noise (standard) deviation and current noise (standard) deviation[19, 20] as per the following formula.

$$R_n = \frac{\sigma_\vartheta}{\sigma_i}$$

$R_p$in the Stern-Geary equation which is inversely proportional to the corrosion, I_{corr} can be calculated as

$$I_{corr} = \frac{b_a . b_c . 1}{2.2\ (b_a + b_c) R_p}$$

Results and Discussion

Polished microstructural images of both C1 and C2 are as represented in Fig. 1, Polishing is performed by using SiC emery (200-1000) grit papers and using a velvet cloth up to the shiny surface. Polishing direction is kept perpendicular to direction of initial

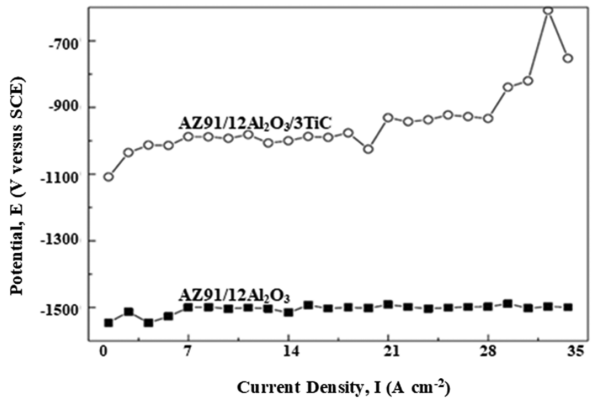

Fig. 2 — Polarization curves for AZ91/12Al_2O_3 and AZ91/12Al_2O_3/3TiC composites in 3.5% NaCl solution

polishing. Each of polished surfaces reveals the distribution of reinforced particles and shape of AZ91 matrix grains developed in the composite. Fig. 1(a) represents the (polished) microscopic surface image of C1 composite. This microscopic image depicts the alpha Mg phase as well as the beta eutectic phase (about 30%) enclosed with Al-rich surrounding and $Al_{12}Mg_{17}$ precipitates. It is also observed that about sixty percent (60% covered with alpha Mg and 40% covered with beta precipitates) of fraction areas have been occupied by the primary phase with minimal grain boundaries near the matrix area. Moreover, Fig. 1(b) depicts the microscopic surface substitution of C2 composite having about fifty percent of the fraction area having the dark zones representing the porosity distribution on the hybrid composite surface and minor particles distribution of base matrix.

Fig. 2 illustrates the results of the polarization test of both the composites when measured in 3.5% NaCl solution. These curves depict only active behaviour with an anodic limiting current and without any passive zone. 0.61 A/cm^2 and 0.18 A/cm^2 are the evaluated values of C1 and C2 composites,

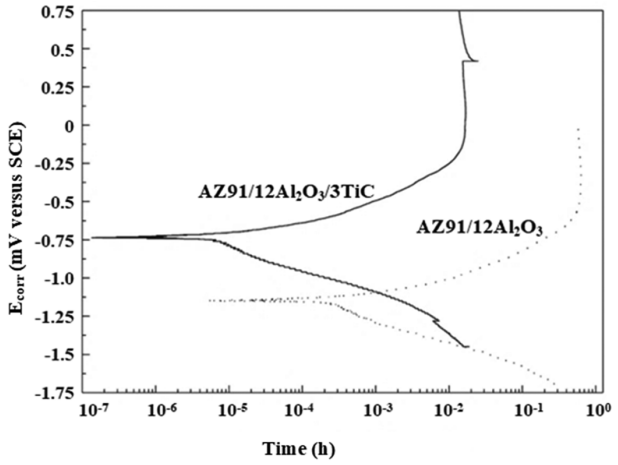

Fig. 3 — Rate of change of E_{corr} value for AZ91/12Al_2O_3 and AZ91/12Al_2O_3/3TiC composites in 3.5% NaCl solution

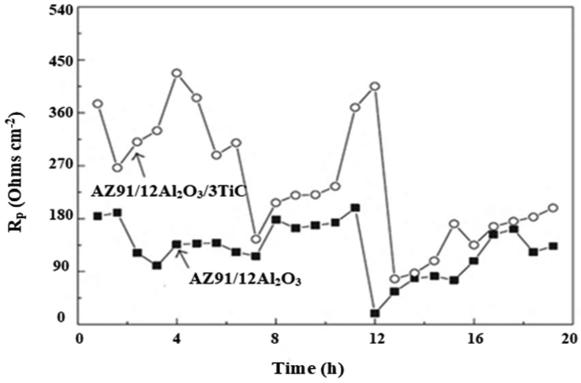

Fig. 4 — Rate of change in *Rp* value with time AZ91 AZ91/12Al_2O_3 and AZ91/12Al_2O_3/3TiC composites in 3.5% NaCl solution

respectively. The results of C1 composite depict E_{corr} having more active behaviour than C2 composites i.e. 982 mV and 580 mV, respectively.

However, the corrosion current density of C2 composite was lower (2.8 X 10^{-3} A cm^2) when compared with C1 composite (1.4X 10^{-4} A cm^2). Fig. 3 demonstrates the change in E_{corr} value with time. The C1 composite retains its more active values in comparison to hybrid composites. After that, Fig. 4 represents the change in *Rp* value with the time of AZ91 Mg composites. The results of Fig. 4 reveal a higher corrosion rate of C1 composites than C2 composites. Initially C1 composite shows a decrease in the corrosion rate but after that an increase in the rate was observed. This indicates the shattering or tearing of the corrosion protective layer and unfolding of the non-protective corrosive layer. This is due to the separation of the alpha Mg phase and enhanced $Al_{12}Mg_{17}$ particles (act as a cathode).

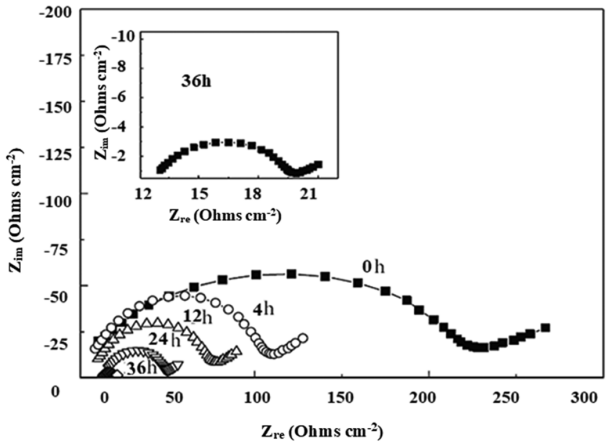

Fig. 5 — Rate of change in Nyquist diagrams for AZ91/12Al_2O_3 in immersion solution

Nyquist diagrams represent capacitive-type depressed semicircles under high frequencies indicating a controlled corrosion process due to the absorption of chloride ions near the immersion solution and AZ91 matrix interfaces. Fig. 5 shows the Nyquist diagrams of C1 composite which shows a capacitive oriented type semicircle under high frequencies but a straight line when frequency decrease. This dipping illustrates a mixed mechanism of corrosion process i.e., transferring of charge from AZ91 metal to its interfaces through a double electrochemical layer. Similarly, during the diffusion process (due to anodic limiting current) shows aggressive ions through the corrosion product layers in the form of polarization curves (Fig. 2). Decremented semicircle type capacitive of C1 composite (with the increase in time period) reveals the high-frequency diameter due to equivalent charge transfer resistance (R_{ct}) and polarization resistance (R_p) as shows above. Similar results (decrease in R_p value) as shown in Fig. 4 i.e., with the increase in time, decrease in R_{ct} value. On the other hand, Fig. 6 shows the Nyquist diagrams of C2 composite. It shows an inductive loop under low frequencies and declining of semicircle diameters as time vanished. This means with the rise of corrosion rate with respect to time, which indicates a non-protective nature of corrosion by-products.

Fig. 7 depicts the time strings of C1 composite for both potential and current. The time strings show a transient curve under high amplitude and then illustrate sudden decrement after a time interval. Each transient string (curve) shows the shattering of the formed corrosion layer with the rise in local current density. But when the time interval increases,

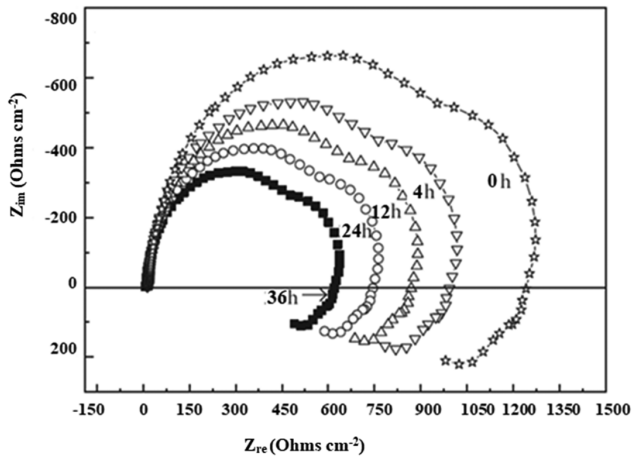

Fig. 6 — Rate of change in Nyquist diagrams for AZ91/12Al_2O_3/3TiC composite in immersion solution

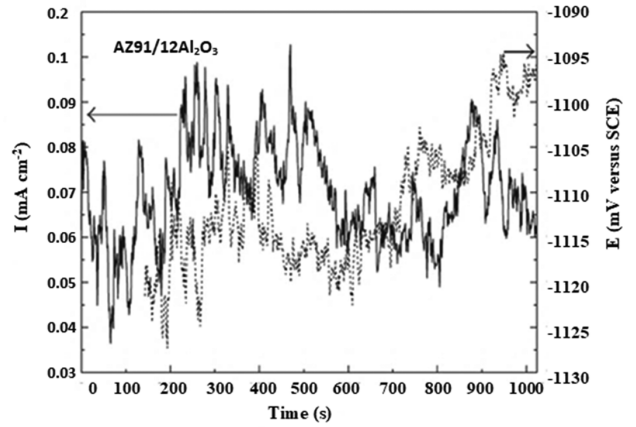

Fig. 7 — Noise examination in current and potential for AZ91/12Al_2O_3 in immersion solution

corrosion starts layering and restoration, then current density decreases. Thus, C1 composite demonstrates high susceptibility towards localized corrosion specifically pitting type. Conversely, the time series of C2 composite shows a transient curve with low intensity which indicates low susceptibility towards pitting type localized corrosion as shown in Fig. 8. To evaluate the localized corrosion of AZ91 Mg composites, the 'Localization Index' factor has been considered, as denoted by L_i[21].

$L_i = \sigma_i i_{rms}$

Where σ_i is the standard current noise deviation value and $i_{rms}$is the current root mean square value.

Both of these values establish a defined range of L_i. L_i range in between 1 and 0.1 then the material results to localized type corrosion. When L_i ranges in between 0.1 to 0.01 then a mixture of both localized and uniform corrosion has been observed. However, if

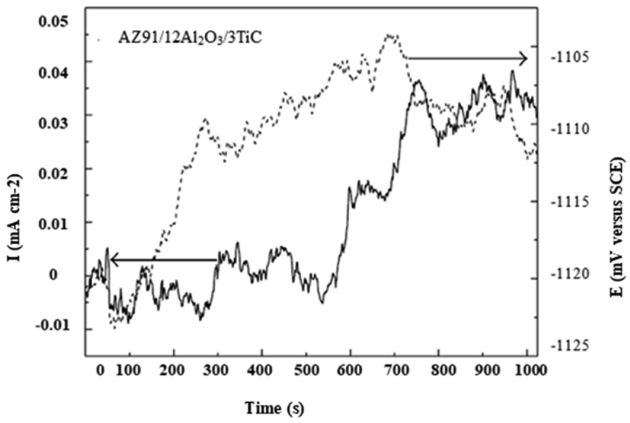

Fig. 8 — Noise examination in current and potential for AZ91/12Al_2O_3/3TiC composite in immersion solution

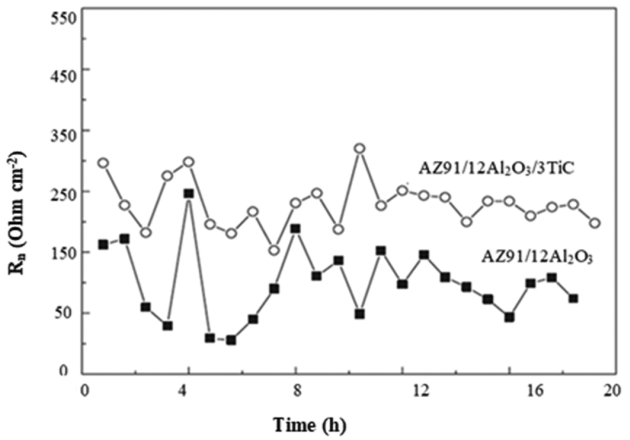

Fig. 9 — Rate of change in the noise resistance value, *Rn*, for AZ91/12Al_2O_3 and AZ91/12Al_2O_3/3TiC composites in immersion solution

L_i lies in-between 0.01 to 0.001, then uniform type corrosion tendency shows. Li values of C1 and C2 composite are 0.2 and 0.1, respectively. From the above results, both composites tend to localized type corrosion but C1 composite is more susceptible to localized degradation.

By dividing the potential noise standard deviation (σ_v) and current noise standard deviation (σ_i), a noise resistance can be calculated (R_n) for both AZ91 Mg composites as shown in Fig. 9, demonstrates a decrease in R_n as time elapsed. C1 composite exhibits low R_n value than C2 composite. Thus, when R_n replaces with R_p (as shown in above formula) C1 composite showed more corrosion rate than hybrid composite. Thus, by analyzing the tool, C2 composite represents a low corrosion rate than C1 composite.

Fig. 10 shows SEM micrographs of corroded C1 and C2 and X-ray diffractogram of corroded C2

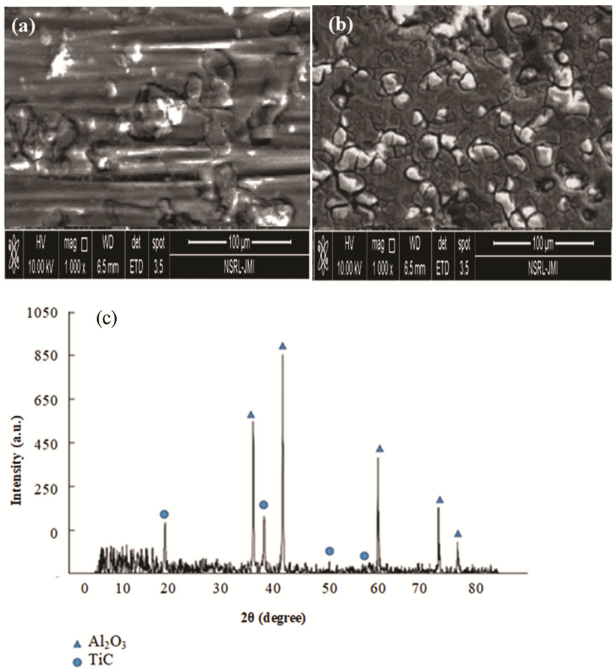

Fig. 10 — SEM micrographs of (a) AZ9112Al_2O_3 and (b) AZ91/12Al_2O_3/3TiC composites, and (c) X-ray diffractogram of AZ91/12Al_2O_3/3TiC composite

composite specimens. The micrograph of C2 (Fig. 10b) shows few corroded particles that detached from the AZ91 Mg matrix. This detachment results in a similar transient curve as shown in Fig. 7. Due to preferential corrosion attack in-between matrix and reinforcing interfaces (TiC and alumina) can be observed due to electrochemical reaction. This electrochemical reaction creates a galvanic effect between alpha Mg, beta Mg, Al Mn inclusions, TiC, and alumina particles. Hence, the development of intermetallic phases under an electrochemical solution induces the existence of micro-galvanic cells. In this micro-galvanic cell, TiC particles and $Al_{12}Mg_{17}$ intermetallic phase behave as cathode whereas alpha-Mg enact as anode. The acceleration of these galvanic cells evaluates the corrosion rate and decrease in corrosion resistance

However, the corroded surface of C1 composite shows porous and cracked layer-type corrosion products. These corrosion products do not allow the electrolyte to pass through metal (AZ91 Mg) and give rise to a transient curve as shown in Fig. 8. Moreover, X-ray diffraction patterns of C1 composite shows $Mg(OH)_2$ and alumina particles as main corrosion products. This is due to the existence of cathodic phases of $Al_{12}Mg_{17}$ particles as shown in Fig. 1. AZ91 Mg matrix and alumina composite interfaces enhance the sensitivity towards hydrolysis reaction. Once the hydrolysis reaction gets started, the corrosion response also proceeds due to the oxidation of Mg as Mg^{2+} and results in $Al_{12}Mg_{17}$ particles as follows:

$$Mg^{2+} + 2OH^- \rightarrow 2Mg(OH)$$

Mg^{2+}ions generates after oxidation of Mg (Mg gives to Mg^{2+}) whereas OH^- releases after oxygen reduction:

$$2H_2O + O_2 + 4e^- \rightarrow 4OH^-$$

These reactions give valid reasons for not detecting the corrosion products due to Mg $(OH)_2$. Due to the insolubility of magnesium hydroxide in the solution, X-ray patterns show the formation of a corrosion product layer at metal/solution interfaces and the withdrawal of un-corroded alumina particles. Similarly, Fig. 2 (as shown in polarization curves), the development of magnesium hydroxide increases the potential and occurrence of diffusion-limiting behaviour of both C1 and C2 composites (as shown in polarization curves).

The results of electrochemical noise measurements of C1 and C2 composites were susceptible to corrosion. Generally, for the initiation of pitting corrosion, there are mainly three steps involved: (1) penetration and then adsorption of chloride ions around oxide surfaces, (2) evolution of soluble hydroxyl aluminum chloride salts, and (3) disintegration of oxide when thinner film exists. However, literature study initially reveals AZ91 Mg based composites majorly depicts the union/ combining of chloride ions[22-25]. The literature study also reported that Mg alloy composites display less corrosion resistance due to the matrix/ reinforcement interfaces acting as potential sites for localized/pitting corrosion[26,27]. In contrast, AZ91 Mg-based hybrid composites report high corrosion resistance and susceptible to localized attack. This is because of the formation of pits and then their growth is restricted due to the presence of reinforcing particles. However, the restricted area offered reduction in the corrosion rate of Mg hybrid composites. In other literature, studies demonstrate the corrosion resistances of the AZ91 matrix remain unchanged with the inclusion of reinforcing particles[28]. However, the galvanizing effects in-between reinforcing (TiC and Alumina) and AZ91 matrix enhanced corrosion rate of AZ91 hybrid composite. In the current study, the formation of an inductive loop depicts in Nyquist curves of C1 composite due to the cohesion of (corrosive) chloride ions around AZ91/NaCl (metal/solution) interfaces. Lastly, C2 composites provides the evidence that

corrosion product layer due to the diffusion of aggressive ions.

Conclusion

By using different electrochemical techniques, AZ91/12Al_2O_3/3TiC composite demonstrates uniform corrosion rate due to the amalgamation of reinforcement particles (TiC and Alumina) and decrements pitting type corrosion resistance in contrast with AZ91/12Al_2O_3 composites. Moreover, both (AZ91/12Al_2O_3 and AZ91/12Al_2O_3/3TiC) AZ91 composites tend to pitting corrosion. However, some galvanic effect is also found between the AZ91 matrix and reinforcing particles of AZ91 Mg hybrid composites. AZ91/12Al_2O_3/3TiC composite evidenced the corrosion rate controlling factor are due to the diffusion of aggressive ions.

References

1 Prasad S S, Prasad S B, Verma K, Mishra R K, Kumar V & Singh S, The role and significance of magnesium in modern day research: A review, *J Magnes Alloy*, 10 (2022) 1.

2 Song J, She J, Chen D & Pan F, Latest research advances on magnesium and magnesium alloys worldwide, *J Magnes Alloy*, 8 (2020) 1.

3 Singh S & Singh K K, A simulation method for the behavior of hybrid Mg-based composite brake caliper in automobile application, In Advances in Mechanical and Materials Technology**,** Edited by Govindan K, Kumar H & Yadav S, (Springer, Singapore, 2022).

4 Singh S & Chauhan N R, Optimization of hardness properties of magnesium-based composites by using Taguchi method In Recent Advances in Mechanical Engineering, Edited by Muzammil M, Chandra A, Kankar P K & Kumar H, (Springer, Singapore, 2021).

5 Parveez B, Kittur M I, Badruddin I A, Kamangar S, Hussien M & Umarfarooq M A, Scientific advancements in composite materials for aircraft applications: A review, *Polymers*, 14 (2022) 5007.

6 Kumar D & Thakur L, Investigation on mechanical and wear performance of ultrasonic-assisted stir cast AZ91D/Al_2O_3 magnesium matrix composites, *Metals Mater Int*, 29 (2023) 2767.

7 Pandya A, Shah M, Pramod B & Srivastava N, A review on heat treatment of magnesium alloys and its effect on various properties, *Adv Mater Sci Metall*, 2022 (2023) 77.

8 Singh S & Chauhan N R, Microstructural and hardness study of stir-casted AZ91D/B4C MMCs, *Int J Microstruct Mater Prop*, 13 (2018) 439.

9 Kumar A, Kumar S, Mukhopadhyay N K, Yadav A & Sinha D K, Effect of TiC reinforcement on mechanical and wear properties of AZ91 matrix composites, *Int J Met*, 16 (2022) 2128.

10 Dubey D, Kadali K, Kancharla H, Zindal A, Jain J, Mondal K & Singh S S, Effect of precipitate characteristics on the corrosion behavior of a AZ80 magnesium alloy, *Metals Mater Int*, 27 (2021) 3282.

11 Bahmani A, Lotfpour M, Taghizadeh M & Kim W J, Corrosion behavior of severely plastically deformed Mg and Mg alloys, *J Magnes Alloy*, 10 (2022) 2607.

12 Aydin F, Sun Y & Emre T M, Influence of TiC content on mechanical, wear and corrosion properties of hot-pressed AZ91/TiC composites, *J Comp Mater*, 54 (2020) 141.

13 Odabasi H K & Odabasi A, Wear and corrosion behavior of Mg-based alloy reinforced with TiC and ZrC particles, *Mater Test*, 62 (2020) 1161.

14 Tarasasanka C, Snehita K, Ravindra K & Sameerkumar D, Optimization of dry sliding wear properties of AZ91E/nano Al_2O_3 reinforced metal matrix composite with grey relational analysis, *Int J Eng Sci Technol*, 11 (2019) 41.

15 Singh A & Bala N, Synthesis and comparative sliding wear behavior of stir cast Mg and Mg/Al_2O_3 metal matrix composites, *Mater Res Exp*, 6 (2019) 076512.

16 Demirdal S & Aydın F, The influence of low-cost eggshell on the wear and electrochemical corrosion behaviour of novel pure Mg matrix composites, *Mater Chem Phys*, 277 (2022) 125520.

17 Singh S & Chauhan N R, Empirical optimization of corrosion rate for magnesium-chromium composites, *Indian J Chem Technol*, 28 (2021) 363.

18 Singh S & Chauhan N R, Influence of B4C on microstructural, mechanical and wear properties of Mg-based composite by two-step stir casting, *Indian J Eng Mater Sci*, 28 (2021) 189.

19 Ciubotariu A C, Benea L, Lakatos-Varsanyi M & Dragan V, Electrochemical impedance spectroscopy and corrosion behaviour of Al_2O_3–Ni nano composite coatings, *Electrochim Acta*, 53 (2008) 4557.

20 Chen Z, Wang W, Liang Q & Lin W, Microstructure and corrosion resistance of electrophoretic deposited carbonated hydroxyapatite-graphene oxide composite coatings on AZ91 magnesium alloy, *Int J Electrochem Sci*, 16 (2021) 211116.

21 Jaquez-Munoz J M, Gaona-Tiburcio C, Cabral-Miramontes J, Nieves-Mendoza, D, Maldonado-Bandala E, Olguin-Coca J & Almeraya-Calderon F, (2021) Electrochemical noise analysis of the corrosion of titanium alloys in NaCl and H2SO4 solutions, *Metals*, 11 (2021) 105.

22 Patle H, Sunil B R & Dumpala R, Machining characteristics, wear and corrosion behavior of AZ91 magnesium alloy fly ash composites produced by friction stir processing, *Mater Sci Eng Technol*, 52 (2021) 88.

23 Xin L V, Kunkun D, Cuiju W, Kaibo N, Quanxin S & Wei L , Effect of SiC size on microstructure and corrosion properties of cast AZ91 Mg-alloys, *J Chin Soc Corros Prot*, 43 (2022) 135.

24 Zang Q, Chen H, Zhang J, Wang L, Chen S & Jin Y, Microstructure, mechanical properties and corrosion resistance of AZ31/GNPs composites prepared by friction stir processing, *J Mater Res Technol*, 14 (2021) 195.

25 Abdollahzadeh A, Bagheri B, Abbasi M, Sharifi F & Moghaddam A O, Mechanical, wear and corrosion behaviors of AZ91/SiC composite layer fabricated by friction stir vibration processing, *Surf Topogr: Metrol Prop*, 9 (2021) 035038.

26 Saranu R, Chanamala R & Putti S R, Corrosion and tribological behavior of magnesium metal matrix hybrid composites: A review, *AIP Conf Proc*, 2259 (2020) 1.

27 Mathiazhagan P & Jayabharathy S, Experimental investigation of mechanical and wear behaviour of AZ91 magnesium hybrid composite materials, Intech Open, (2022).

28 Dani M S, Dave I B & Parmar B, Corrosion behavior of die-cast and friction stir-processed AZ91 magnesium alloys in 5% NaCl, *J Inst Eng (India): Ser D*, 100 (2019) 21.